EurJIC European Journal of Inorganic Chemistry
ChemPubSoc Europe
FULL PAPER

DOI:10.1002/ejic.201402060

Compressed CO_2 Accelerated the Synthesis of Mesoporous Heteroatom-Substituted Aluminophosphates for Enhanced Catalytic Activity

Fangxiao Wang,[a] Lin Liang,[b,c] Jun Ma,[b] Lei Shi,[a] and Jianmin Sun*[a,b]

Keywords: Heterogeneous catalysis / Mesoporous materials / Aluminium / Zeolites / Oxidation

AFI-structured zeolites of aluminophosphates AlPO-5 and heteroatom-substituted aluminophosphates MeAPO-5 (Me = Fe, Co) have been synthesized in the presence of compressed CO_2, the synthesized materials exhibiting mesoporosity without the use of additional mesotemplates. The mesoporosity was introduced by CO_2-in-water emulsions acting as mesotemplate during the crystallization of the zeolites. In addition, the crystallization time was shortened in compressed CO_2 compared with the conventional synthesis in the absence of CO_2. The synthesized aluminophosphates MeAPO-5 (Me = Fe, Co) displayed much higher activities in the oxidation of styrene than conventional aluminophosphates MeAPO-5 (Me = Fe, Co) due to the presence of mesopores in the former catalysts, which favor the diffusion of reactants and products. The compressed CO_2 method provides a simple, green, and economic route to hierarchical zeolites, which are of great importance for industrial applications.

Introduction

Zeolites are extensively employed in the fields of adsorption, separation, and heterogeneous catalysis because of their intrinsic properties such as high surface area, narrow micropore distribution, high thermal stability, and capacity for being doped by different heteroatom ions, which generates heterogeneous active sites within structures with shape-selective ability.[1] However, their relatively small and uniform micropores strongly influence the mass transfer of reactants and products, reducing the catalytic conversion of bulky molecules. Recently, the synthesis of mesoporous zeolites, which possess both the advantages of mesoporous materials and zeolites, has been the focus of attention for solving the existing shortcomings of zeolites. Successful examples of the synthesis of mesoporous zeolites are the use of a mixture of various mesoscale templates with a zeolite precursor. Mesoscale templates such as mesoporous carbon,[2–7] organic/inorganic hybrid surfactants,[8] silylated polymers,[9] and mesoscale cationic polymers[10,11] have commonly been used. The templates are then removed by calcination after hydrothermal treatment to produce mesopores within the zeolite crystals. For example, Srivastava et al. synthesized nanocrystalline MFI zeolites with intracrystal mesopores by using alkyltriethoxysilane as template.[12] Yang and Zhou and their co-workers reported the synthesis of hierarchical and metal-substituted AlPO-5 by using glucose as the mesoporous template.[13,14] However, the high cost of the organic templates for the formation of mesoporosity and the complexity of the synthetic procedures limit the far-ranging applications of these mesoporous zeolites on an industrial scale. Therefore, the challenges associated with the synthesis of hierarchical porous materials by facile and economic routes continue to be of great importance.

Supercritical or compressed CO_2 has attracted considerable attention in recent years because of its availability, low cost, nonflammability, and low toxicity, and it has been widely used in different fields, such as extraction and fractionation,[15] chemical reactions,[16–19] and materials science,[20,21] among others.[22,23] To date, there have been a few successful examples of the preparation of porous materials in the presence of compressed CO_2.[24–28] Ming et al. synthesized porous, hollow biphase γ-/α-Fe_2O_3 nanoparticles in CO_2-expanded ethanol solution,[27] mesoporous silica hollow spheres were prepared from CO_2-in-water emulsion-templating in the presence of non-ionic block copolymers,[28] and our group reported the synthesis of MFI zeolites ZSM-5 in compressed CO_2 for the first time. Moreover, mesoporosity has been generated in crystalline MFI zeolites

[a] Natural Science Research Center, The Academy of Fundamental and Interdisciplinary Science, Harbin Institute of Technology, Harbin 150080, China
[b] State Key Laboratory of Urban Water Resources and Environment, Harbin Institute of Technology, Harbin 150090, China
E-mail: sunjm@hit.edu.cn
http://homepage.hit.edu.cn/pages/sunjianmin
[c] School of Life Sciences and Technology, Harbin Institute of Technology, Harbin 150080, China

without the use of any mesoscale organotemplate, and the mesopore volume could be adjusted by changing the pressure of CO_2.[29] Thus, the use of compressed CO_2 has led to a new route for the simple and economic synthesis of mesoporous zeolites. In our continuing efforts to prepare porous materials by novel methods, we report herein the successful synthesis of AFI-structured aluminophosphates AlPO-5 and heteroatom-substituted aluminophosphates MeAPO-5 with improved crystallization rates and mesoporosity in compressed CO_2 without the use of any mesoscale templates. As a result of the presence of mesopores in Fe- and Co-doped AlPO-5, the increased rate of mass transfer of reactants and products has led to an improvement in the catalytic activity and selectivity of these materials in the oxidation of styrene compared with ordinary Fe- and Co-doped AlPO-5 materials synthesized in the absence of CO_2. The formation of mesoporosity in aluminophosphates synthesized in compressed CO_2 is apparently related to the presence of CO_2-in-water emulsions as mesotemplate, which was confirmed by the absence of mesoporosity in AlPO-5 synthesized in the presence of N_2 and in the absence of compressed CO_2 in control experiments.

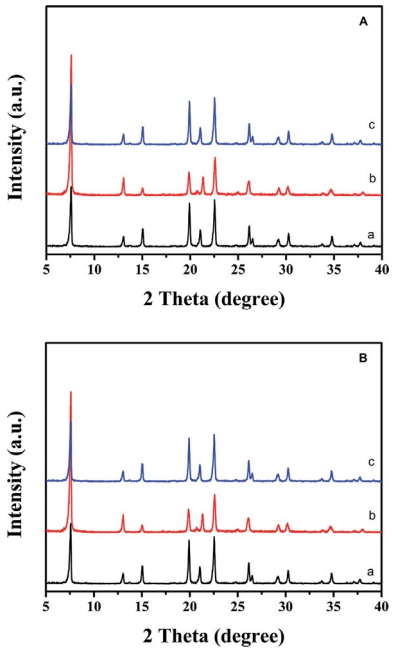

Figure 1. XRD patterns of (A) as-synthesized and (B) calcined samples of (a) C-AlPO-5, (b) AlPO-8-28, and (c) AlPO-10-15 (AlPO-*x*-*y*: *x* and *y* represent the CO_2 pressure and crystallization time).

Results and Discussion

The powder XRD patterns of the as-synthesized AlPO-5 samples are shown in Figure 1A. All the AlPO-5 samples exhibited diffraction peaks at 2θ values of 7.5, 12.9, 15.0, 19.8, 21.0, and 22.5°, which were assigned to the AFI structure of AlPO-5.[30] No peaks from other crystalline phases were observed, which indicates that AlPO-5 zeolites were successfully synthesized in compressed CO_2. Moreover, the diffraction peaks did not change after calcination at 550 °C (Figure 1B), which suggests that the AlPO-5 samples synthesized in compressed CO_2 possess high thermal stability. Noticeably, it only took 28 h for the crystallization of AlPO-5 samples at a CO_2 pressure of 8 MPa. This crystallization time is markedly shorter than the 48 h required for the crystallization of conventional AlPO-5 in the absence of compressed CO_2. Furthermore, the crystallization time was further reduced to 15 h when the CO_2 pressure was increased to 10 MPa, which indicates that compressed CO_2 favors the fast crystallization of AFI zeolites. Similar enhancements of crystallization rates have been observed in the synthesis of MFI zeolites.[29] The pH of the reaction gel played a crucial role in the synthesis of the AFI zeolites. The pH of the starting gel was 6.70 and decreased to 5.62 after crystallization in compressed CO_2 at 8 MPa, which is in the range of the optimum pH for the synthesis of AlPO-5 zeolites. The pH decreased as a result of the dissolution of CO_2 in water and its partial ionization to form the acid.[29]

Figure 2 shows the nitrogen isotherms of the calcined AlPO-5 samples. A steep increase in the isotherms can be seen at relative pressures P/P_0 in the range of 0.4–1.0 in the samples of AlPO-5 synthesized in compressed CO_2, which is characteristic of the presence of mesopores. In contrast, there were no obvious hysteresis loops in the C-AlPO-5 sample synthesized in the absence of compressed CO_2 and the N-AlPO-5 sample synthesized in N_2. These results indicate that the formation of mesoporosity in AlPO-5 zeolites is strongly related to the use of compressed CO_2. The textural properties of the calcined AlPO-5 samples are summarized in Table 1. Notably, the mesoporous volume is significantly influenced by CO_2 pressure, as it increases remarkably from 0.03 to 0.15 cm^3/g with CO_2 pressure increasing from 8 to 10 MPa. However, the microporous volume decreased markedly, further confirming that compressed CO_2 is a key factor for the formation of mesoporosity. Because of the decrease in microporosity, the BET surface area decreased from 104.5 to 66.2 m^2/g with increasing CO_2 pressure. Correspondingly, the mesopore size distributions were estimated to be around 30–50 nm by applying the BJH method. Before the use of CO_2 pressure, micelles were

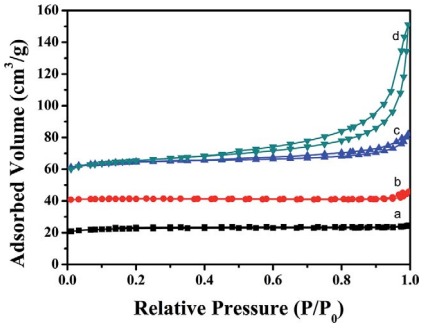

Figure 2. Nitrogen isotherms of calcined samples of (a) C-AlPO-5, (b) N-AlPO-5, (c) AlPO-8-28, and (d) AlPO-10-15. The isotherms for (b), (c), and (d) are offset by 20, 40, and 40 cm^3/g, respectively, along the vertical axis for clarity.

formed by using the protonated triethylamine (TEA) template, which provided steric support for the microporous channel of AFI zeolites through their specific molecular vibrations in the early stages.[31] When the autoclave was purged with compressed CO_2, the gas quickly spread and partly dissolved in the water of the gel around the TEA micelles to form CO_2-in-water emulsions. Moreover, the CO_2-in-water emulsions were stabilized by the TEA microporous-structured micelles. The existence of CO_2-in-water emulsions was proved by the phase behavior of the gel observed in our previous work.[29] The introduction of mesopores possibly results from the CO_2-in-water emulsions, which act as mesoporous templates with TEA micelles acting as microporous templates. After crystallization, TEA was removed by calcination, and CO_2 was depressurized, and thus mesopores were introduced into the zeolite crystal. Porous materials synthesized from such CO_2-in-water emulsions have also been reported.[32,33]

Table 1. Textural parameters of the calcined AlPO-5 samples.

Sample	S_{BET}[a] [m²/g]	V_{meso}[b] [cm³/g]	V_{micro}[c] [cm³/g]	D_{meso}[d] [nm]
C-AlPO-5	113.8	0.002	0.055	–
N-AlPO-5	21.4	0.007	0.010	–
AlPO-8-28	104.5	0.034	0.044	30–50
AlPO-10-15	66.2	0.150	0.015	30–50

[a] BET surface area. [b] Mesoporous volume. [c] Microporous volume. [d] Mesopore size distribution calculated from the desorption branch by the BJH method.

The presence of mesopores in the AlPO-5 sample is directly evidenced by bright parts in the TEM image (Figure 3). Previously reported mesoporous AlPO-5 zeolites were synthesized by using mesoscale templates.[7,13] However, in this work, we show the synthesis of mesoporous AlPO-5 zeolites in pressurized CO_2 without the use of any mesoscale organotemplate. As organic mesoporous templates are not used during the synthesis, this novel synthetic process is attractive for its cost-effective and environmentally benign features.

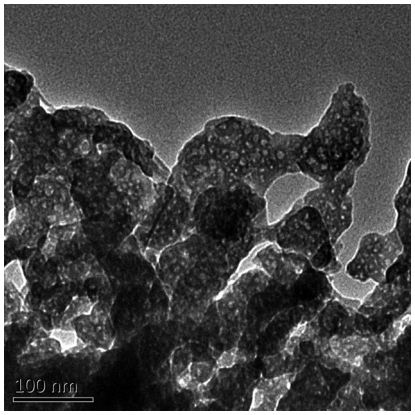

Figure 3. TEM image of the AlPO-5 sample.

Solid-state NMR measurements provided convincing evidence for the coordination environment of aluminium. The ^{27}Al MAS NMR spectra of calcined AlPO-5 samples are shown in Figure 4. All the AlPO-5 samples were fully hydrated and display two peaks at δ = 37 and –11 ppm. The intense signal at $\delta \approx 37$ ppm has been ascribed to the tetrahedral Al species in the AFI structure and the resonance peak at at $\delta \approx -11$ ppm has been assigned to hexacoordinate Al, which indicates that the AlPO-5 sample is composed of AlO_4 and AlO_6 units.[34,35]

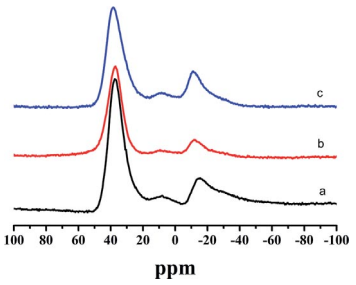

Figure 4. Solid-state ^{27}Al MAS NMR spectra of calcined samples of (a) C-AlPO-5, (b) AlPO-8-28, and (c) AlPO-10-15.

Compared with AlPO-5, heteroatom-substituted mesoporous aluminophosphates generate catalytic redox or acid sites.[14] The powder XRD patterns of calcined FeAPO-5 and CoAPO-5 samples are shown in Figure 5. All the diffraction peaks of the samples can be assigned to AFI-structured AlPO-5 with no specific signals of metal oxide compounds being observed, which indicates that the samples are thermally stable, and the doped metals do not change the structure of AlPO-5. The FeAPO-5 and CoAPO-5 samples crystallized within 28 h at 8 MPa; however, it took 48 h for the crystallization of conventional MeAPO-5, which suggests that the compressed CO_2 favors the fast crystallization process.

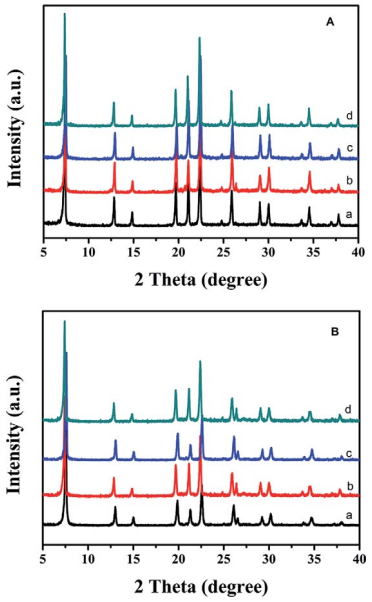

Figure 5. XRD patterns of calcined samples of (A) FeAPO-5 and (B) CoAPO-5. (a) C-MeAPO-5, (b) MeAPO-5 (0.04), (c) MeAPO-5 (0.08), and (d) MeAPO-5 (0.12). For the meaning of the numbers in parentheses, see footnotes [c] and [d] in Table 2.

Figure 6 shows the nitrogen isotherms of the MeAPO-5 samples. The MeAPO-5 samples synthesized in compressed CO_2 exhibit typical type IV adsorption curves. A steep increase can be seen at relative pressures P/P_0 in the range of 0.4–1.0 in the samples of FeAPO-5, ascribed to the presence of mesopores. In contrast, conventional FeAPO-5 displays no hysteresis loop in this range. The BET surface area of the FeAPO-5 sample synthesized in compressed CO_2 is 76 m^2/g, and its mesoporous volume is 0.20 cm^3/g (Table 2). The reduced surface area is related to the loss of microporosity compared with conventional FeAPO-5. Similarly, CoAPO-5, which also possesses mesopores, shows characteristic type IV isotherms, and its BET surface area was reduced to 120 m^2/g due to the presence of mesopores, as compared with 260 m^2/g for conventional CoAPO-5, and the mesoporous volume is 0.30 cm^3/g (Table 2). Correspondingly, the mesopore size distributions were estimated to be around 20–60 nm by applying the BJH method. The bright parts of the TEM images of the calcined FeAPO-5 and CoAPO-5 samples give clear evidence for the existence of mesopores (Figure 7), consistent with the results of the nitrogen isotherms.

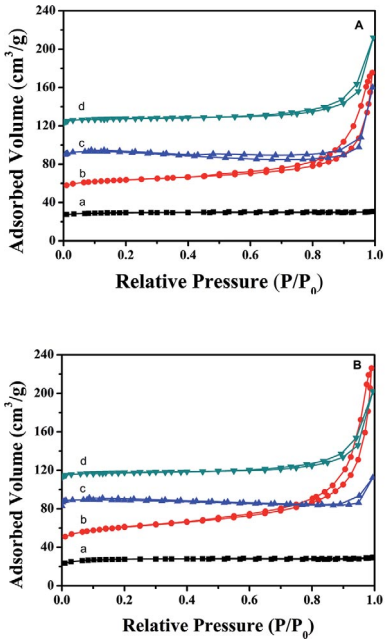

Figure 6. Nitrogen isotherms of calcined samples of (A) FeAPO-5 and (B) CoAPO-5. (a) C-MeAPO-5, (b) MeAPO-5 (0.04), (c) MeAPO-5 (0.08), and (d) MeAPO-5 (0.12). The isotherms for (b), (c), and (d) are offset by 30, 60, and 90 cm^3/g, respectively, along the vertical axis for clarity. For the meaning of the numbers in parentheses, see footnotes [c] and [d] in Table 2.

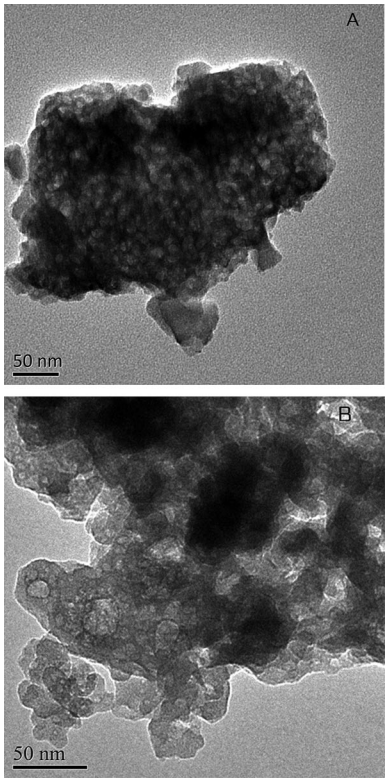

Figure 7. TEM images of calcined (A) FeAPO-5 and (B) CoAPO-5 samples.

UV/Vis spectroscopy is a powerful tool for characterizing the substitution of heteroatoms in aluminophosphates. Figure 8 shows the UV/Vis spectra of the as-synthesized and calcined Fe- and Co-substituted aluminophosphates. The spectra of the as-synthesized FeAPO-5 samples show a strong broad peak at 280 nm and a weak shoulder at 470 nm [Figure 8A (a) and (b)]. The peak at 280 nm has been assigned to Fe^{3+} species in a tetrahedral network, and the peak at 470 nm has been attributed to octahedral iron species.[36,37] The spectra of the calcined FeAPO-5 samples show no obvious difference to those of the as-synthesized samples. The as-synthesized CoAPO-5 samples show four absorption peaks at 480, 540, 580, and 626 nm [Figure 8B (a) and (b)]. The peak at 626 nm has been assigned to tetra-

Table 2. Textural parameters of calcined MeAPO-5 samples.

Sample	S_{BET}[a] [m^2/g]	V_{meso}[b] [cm^3/g]	$S_{Me/Al/P}$[c] (molar ratio)	$F_{Me/Al/P}$[d] (molar ratio)
C-FeAlPO-5	88	0.004	0.04:0.96:1	0.03:0.92:1
FeAPO-5 (0.04)	76	0.20	0.04:0.96:1	0.04:0.84:1
FeAPO-5 (0.08)	135	0.17	0.08:0.92:1	0.08:0.90:1
FeAPO-5 (0.12)	27	0.14	0.12:0.88:1	0.11:0.89:1
C-CoAPO-5	260	0.006	0.04:0.96:1	0.03:0.91:1
CoAPO-5 (0.04)	120	0.30	0.04:0.96:1	0.04:0.85:1
CoAPO-5 (0.08)	125	0.09	0.08:0.92:1	0.04:0.91:1
CoAPO-5 (0.12)	19	0.13	0.12:0.88:1	0.13:0.89:1

[a] BET surface area. [b] Mesoporous volume. [c] Me/Al/P (molar ratio) in the starting gels. [d] Me/Al/P (molar ratio) in the final products.

hedral coordination, and the peak at around 540 nm has been attributed to the octahedral Co^{2+} species. The peak at 480 nm indicates the presence of octahedrally coordinated extra-framework Co^{2+} species.[36] However, the calcined CoAPO-5 samples show one broad peak between 450 and 700 nm, which also suggests the existence of tetrahedral and octahedral coordinated cobalt.[38]

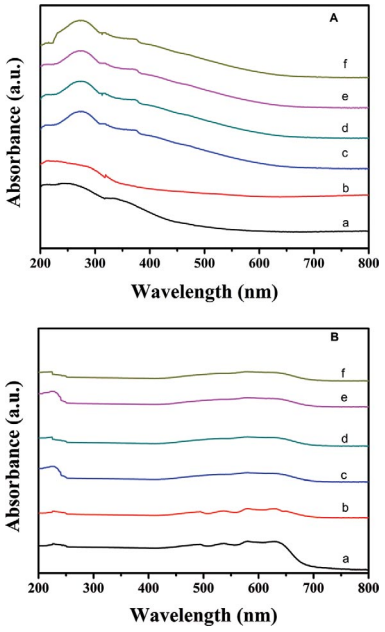

Figure 8. UV/Vis spectra for samples of (A) FeAPO-5 and (B) CoAPO-5. (a) As-synthesized C-MeAPO-5, (b) as-synthesized MeAPO-5 (0.04), (c) calcined C-MeAPO-5, (d) calcined MeAPO-5 (0.04), (e) calcined MeAPO-5 (0.08), and (f) calcined MeAPO-5 (0.12).

Temperature-programmed desorption of ammonia (NH_3-TPD) was used to investigate the acid properties of the samples (Figure 9). For AlPO-5, a desorption peak can be seen at around 100 °C, which corresponds to the weak acid site caused by Al^{3+} in the framework.[39] In the C-MeAPO-5 sample, the low-temperature peaks at around 100 °C are stronger, which implies that the introduction of metal atoms into the AlPO-5 framework leads to an increase in the number of weak acid sites. In the case of FeAPO-5 and CoAPO-5, synthesized in compressed CO_2, the peaks arising from the weak acid sites tend to shift to a higher temperature, around 150 °C, which suggests that their acid strengths are higher than those of the C-MeAPO-5 samples synthesized in the absence of CO_2.[40]

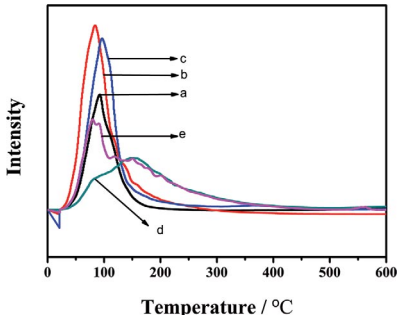

Figure 9. NH_3-TPD profiles for calcined samples of (a) AlPO-5, (b) C-FeAPO-5, (c) C-CoAPO-5, (d) FeAPO-5, and (e) CoAPO-5.

Moreover, to determine the surface chemical states of the metals in the MeAPO-5 samples, XPS measurements were carried out. Peaks ascribed to Fe $2P_{3/2}$ and Fe $2P_{1/2}$ are observed at binding energies of 712.8 and 726.4 eV, respectively (Figure 10A). The Fe $2P_{3/2}$–Fe $2P_{1/2}$ peak separation is approximately 13.6 eV, which indicates the presence of Fe^{3+} species in the FeAPO-5 sample.[41] In the case of CoAPO-5, the incorporation of Co^{2+} was confirmed by the typical characteristic peaks of Co $2P_{3/2}$ and Co $2P_{1/2}$ at 782.7 and 796.6 eV, respectively (Figure 10B). These results are in good agreement with the results of the UV/Vis characterizations.[42]

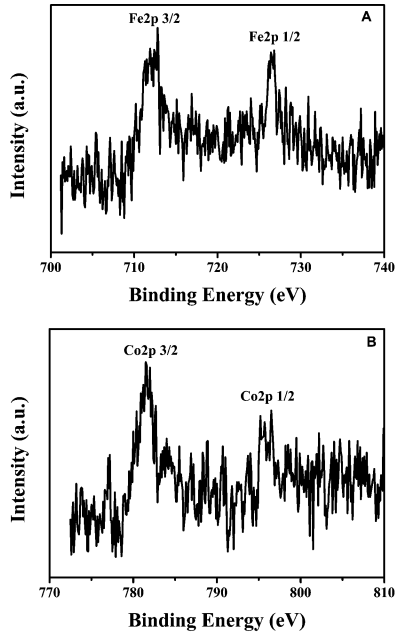

Figure 10. (A) Fe 2P and (B) Co 2P XPS spectra of the MeAPO-5 (0.04) samples.

It is well known that Fe- and Co-substituted zeolites are active in catalytic oxidation reactions. In this paper, the oxidation of styrene by *tert*-butyl hydroperoxide (TBHP), which is of great scientific and technological importance, was employed as a model reaction to test the catalytic properties of these zeolites. The results are presented in Table 3. In the blank experiment, the conversion of styrene was low at 10.6% without any catalyst. With C-FeAPO-5 and C-CoAPO-5 as catalysts, the conversions increased to 51.4 and 59.8%, respectively, which indicates that Fe and Co are the active sites in the oxidation reaction. Noticeably, the conversion and selectivity to styrene oxide increased significantly with mesoporous MeAPO-5 catalysts. The styrene conversion increased to 72.1% with FeAPO-5 and to 78.9% with CoAPO-5. Correspondingly, the selectivity to styrene oxide was enhanced to 24.9 and 26.1%, respectively, and the selectivity to phenylacetaldehyde decreased. In addition to the oxidation properties of the metal-doped AlPO-5 cata-

lysts, the acidity of the catalysts also had effects on the activity and product selectivity. The enhanced catalytic activity and selectivity in the oxidation of styrene to styrene oxide may be related to the greater acidity in the MeAPO-5 samples compared with the C-MeAPO-5 samples, as observed by NH_3-TPD, which favors the epoxidation of styrene to styrene oxide and hinders the isomerization of styrene oxide to phenylacetaldehyde (Scheme 1). Although the oxidation of styrene is not a diffusion-controlled reaction, considering the similar crystal sizes (within 0.5–1 μm), textural parameters, and crystallinity of MeAPO-5 to microporous conventional MeAPO-5, the high catalytic activity over MeAPO-5 has been assigned to the presence of hierarchical mesoporosity in the sample, which may accelerate the mass transport of reactants and products in the oxidation of styrene.

Table 3. Catalytic activity in styrene oxidation reactions over various catalysts.[a]

Catalyst	Conversion [%]	Selectivity [%]			
		SO	BA	PA	Others
Without	10.6	5.9	28.1	0.9	65.1
C-FeAPO-5	51.4	15.9	52.6	13.5	18.0
FeAPO-5 (0.04)	72.1	24.9	65.1	2.6	7.4
FeAPO-5 (0.08)	78.5	31.6	52.1	4.4	11.9
FeAPO-5 (0.12)	82.4	56.4	39.5	2.2	1.9
C-CoAPO-5	59.8	18.7	58.8	11.4	11.1
CoAPO-5 (0.04)	78.9	26.1	63.2	2.1	8.6
CoAPO-5 (0.08)	81.8	35.6	48.3	5.2	10.9
CoAPO-5 (0.12)	85.4	59.9	32.6	3.4	4.1

[a] Reaction conditions: catalyst (90.1 g), styrene (10 mmol), TBHP (15 mmol), 60 °C, 3 h. SO = styrene oxide; BA = benzaldehyde; PA = phenylacetaldehyde; Others = acids etc.

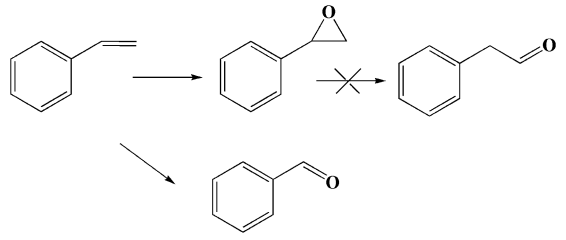

Scheme 1. Proposed reaction routes in the epoxidation of styrene over MeAPO-5.

Conclusions

AFI-structured aluminophosphates and heteroatom-substituted aluminophosphates with mesoporosity have been successfully synthesized in the presence of compressed CO_2. The mesoporosity formed in these zeolites is related to the presence of CO_2-in-water emulsions acting as templates. Moreover, the crystallization time was shortened in the presence of compressed CO_2. Owing to the existence of mesopores, Fe- and Co-substituted AlPO-5 catalysts displayed higher activity in the oxidation of styrene than conventional catalysts obtained in the absence of compressed CO_2. The compressed CO_2 approach provides a simple, green, and economic procedure for the synthesis of mesoporous zeolites, which are of great importance for industrial applications of reactions involving bulky molecules.

Experimental Section

Preparation of AFI-Structured Mesoporous AlPO-5 Zeolites in Compressed CO_2: Aluminium triisopropoxide [Al(O*i*Pr)$_3$], orthophosphoric acid (H_3PO_4), triethylamine (TEA), hydrofluoric acid (HF), ferric nitrate nonahydrate [$Fe(NO_3)_3 \cdot 9H_2O$], and cobalt nitrate hexahydrate [$Co(NO_3)_2 \cdot 6H_2O$] were of AR purity.

In a typical run for the synthesis of aluminophosphate AlPO-5 in compressed CO_2, first, Al(O*i*Pr)$_3$ (4.184 g) was dissolved in deionized water (18 g), then dilute H_3PO_4 (0.196 g) and TEA (0.304 g) were added dropwise, and the mixture was stirred at ambient temperature for 2 h. Then dilute HF solution (8 mg) was added with continuous stirring for a further 2 h, and subsequently the mixture was transferred to a 50 mL stainless-steel autoclave. The molar composition of the starting gel was Al/P/TEA/HF/H_2O = 1.0:1.0:1.5:0.2:50. The 50 mL autoclave was heated to 170 °C, pressurized with CO_2 up to 8 MPa, and crystallization occurred at 170 °C for 28 h. CO_2 was introduced into the free volume over the liquid gel, but during the reaction process, some CO_2 dissolved in the liquid gel to form a CO_2-in-water emulsion as the mesoporous template. Furthermore, the gel was not moved during the crystallization, and after the crystallization, the CO_2 in and above the gel was released by depressurization. Finally, the solid products were separated by filtration, dried at room temperature, and calcined at 550 °C for 6 h. The samples were designated as AlPO-*x*-*y*, in which *x* and *y* represent the CO_2 pressure and crystallization time, respectively.

Heteroatom-substituted aluminophosphates MeAPO-5 (Me = Fe, Co) were synthesized similarly in the presence of $Fe(NO_3)_3 \cdot 9H_2O$ or $Co(NO_3)_2 \cdot 6H_2O$ with starting gel molar compositions of Al/Me/P/TEA/HF/H_2O = (1 – *n*):*n*:1.0:1.5:0.2:50. The sample was designated as MeAPO-5 (*n*), in which *n* represents the amount of metal added. The autoclave was pressurized with CO_2 up to 8 MPa, and the samples crystallized at 170 °C for 28 h. Finally, the solid products were separated, dried and calcined at 550 °C for 6 h.

For comparison, conventional syntheses of AlPO-5 and MeAPO-5 (Me = Fe, Co) in the absence of compressed CO_2 were synthesized as reported in the literature at 180 °C for 48 h[43,44] and designated as C-AlPO-5 and C-MeAPO-5. To investigate the effect of atmosphere on the structures of the zeolites, AlPO-5 was synthesized at 170 °C for 28 h under N_2 instead of CO_2 and designated as N-AlPO-5.

Characterizations: Powder X-ray diffraction (PXRD) analysis was performed with a Bruker D8 Advance X-ray powder diffractometer with Cu-K_α radiation (40 kV, 40 mA). Nitrogen adsorption/desorption isotherms were measured at –196 °C with an ASAP 2020 volumetric analyzer. Before analysis, the samples were outgassed at 200 °C under vacuum for 12 h. The surface areas were calculated by using the Brunauer–Emmett–Teller (BET) method, and the total pore volumes were determined from the amount of nitrogen adsorbed at $P/P_0 \approx 0.99$. TEM experiments were performed with a Tecnai G2 Spririt electron microscope with an acceleration voltage of 120 kV. The sample compositions were determined by inductively coupled plasma (ICP) using a Perkin–Elmer plasma 40 emission spectrometer. Solid-state NMR experiments were performed with a Varian Infinity plus-400 spectrometer equipped with a 4 mm magic angle spinning (MAS) probe. ^{27}Al MAS NMR spectra were

recorded with $Al(H_2O)_6^{3+}$ as external standard reference at a resonance frequency of 104.2 MHz and a spinning rate of 10 kHz. UV/Vis spectra were recorded with a Perkin–Elmer Lambda 750 spectrometer in the range of 200–800 nm. Temperature-programmed desorption of ammonia (NH_3-TPD) experiments were performed with a chemisorption analyzer (Quanta-chrome ChemBet 300). X-ray photoelectron spectroscopy (XPS) was performed with a Phi Quantera spectrometer using Al-K_α X-rays as the excitation source.

Catalysis of Styrene Oxidation: AR-grade styrene and *tert*-butyl hydroperoxide (70% solution, TBHP) were used in the oxidation reactions. In a standard run, styrene (10 mmol) and catalyst (0.1 g) were mixed in a 50 mL glass reactor and heated to the given temperature. TBHP (15 mmol) was then added to the reactor. After heating the mixture at 60 °C for 3 h, the products were removed and analyzed by gas chromatography (Agilent 6890) using a flame ionization detector. The identities of the products were also confirmed by using standard samples and GC–MS (Agilent 6890) with helium as the carrier gas.

Acknowledgments

We sincerely acknowledge the financial support from the National Natural Science Foundation of China (21073049, 21373069), the New Century Excellent Talents in University (NCET-10-0064), the State Key Laboratory of Urban Water Resources and Environment of the Harbin Institute of Technology (HIT2013TS01), the Open Fund of the Key Laboratory of Functional Inorganic Materials Chemistry (Heilongjiang University) and the Fundamental Research Funds of the Central Universities (HIT IBRSEM 201327).

[1] A. Corma, *Chem. Rev.* **1997**, *97*, 2373–2420.
[2] C. H. Jacobsen, C. Madsen, J. Houzvicka, I. Schmidt, A. Carlsson, *J. Am. Chem. Soc.* **2000**, *122*, 7116–7117.
[3] Y. Tao, H. Kanoh, K. Kaneko, *J. Am. Chem. Soc.* **2003**, *125*, 6044–6045.
[4] Z. Yang, Y. Xia, R. Mokaya, *Adv. Mater.* **2004**, *16*, 727–733.
[5] H. C. Li, Y. Sakamoto, Z. Liu, T. Ohsuna, O. Terasaki, M. Thommes, S. Che, *Microporous Mesoporous Mater.* **2007**, *106*, 174–179.
[6] Y. M. Fang, H. Q. Hu, *J. Am. Chem. Soc.* **2006**, *128*, 10636–10637.
[7] K. Egeblad, M. Kustova, S. K. Klitgaard, K. Zhu, C. H. Christensen, *Microporous Mesoporous Mater.* **2007**, *101*, 214–223.
[8] M. Choi, H. S. Cho, R. Srivastava, C. Venkatesan, D. H. Choi, R. Ryoo, *Nat. Mater.* **2006**, *5*, 718–723.
[9] H. Wang, T. J. Pinavaia, *Angew. Chem. Int. Ed.* **2006**, *45*, 7603–7606; *Angew. Chem.* **2006**, *118*, 7765.
[10] F. S. Xiao, L. F. Wang, C. Y. Yin, K. F. Lin, Y. Di, J. X. Li, R. R. Xu, D. S. Su, R. Schlögl, T. Yokoi, T. Tatsumi, *Angew. Chem. Int. Ed.* **2006**, *45*, 3090–3093; *Angew. Chem.* **2006**, *118*, 3162.
[11] L. F. Wang, Z. Zhang, C. Y. Yin, Z. C. Shan, F. S. Xiao, *Microporous Mesoporous Mater.* **2010**, *131*, 58–67.
[12] R. Srivastava, N. Iwasa, S. I. Fujita, M. Arai, *Chem. Eur. J.* **2008**, *14*, 9507–9511.
[13] X. M. Yang, T. L. Lu, C. Chen, L. P. Zhou, F. Wang, Y. L. Su, J. Xu, *Microporous Mesoporous Mater.* **2011**, *144*, 176–182.
[14] L. P. Zhou, T. L. Lu, J. L. Xu, M. Z. Chen, C. F. Zhang, C. Chen, X. M. Yang, J. Xu, *Microporous Mesoporous Mater.* **2012**, *161*, 76–83.
[15] S. C. Li, Z. Wang, X. W. Yu, J. X. Wang, S. C. Wang, *Adv. Mater.* **2012**, *24*, 3196–3200.
[16] M. Caravati, J. D. Grunwaldt, A. Baiker, *Phys. Chem.* **2005**, *7*, 278–285.
[17] X. Wang, N. S. Venkataramanan, H. Kawanami, Y. Ikushima, *Green Chem.* **2007**, *9*, 1352–1355.
[18] R. Mello, A. Olmos, J. P. Carbonell, M. G. Nunez, G. Asensio, *Green Chem.* **2009**, *11*, 994–999.
[19] T. Seki, A. Baiker, *Chem. Rev.* **2009**, *109*, 2409–2454.
[20] S. Livi, J. Duchet-Rumeau, J. F. Gérard, *J. Colloid Interface Sci.* **2012**, *369*, 111–116.
[21] J. Ming, H. Y. Cheng, Y. C. Yu, Y. Q. Wu, F. Y. Zhao, *J. Mater. Chem.* **2011**, *21*, 6654–6659.
[22] J. L. Zhang, B. X. Han, C. X. Zhang, W. Li, X. Y. Feng, *Angew. Chem. Int. Ed.* **2008**, *47*, 3012–3015; *Angew. Chem.* **2008**, *120*, 3054.
[23] M. Poliakoff, J. M. Fitzpatrick, T. R. Farren, P. T. Anastas, *Science* **2002**, *297*, 807–810.
[24] Y. J. Zhao, J. L. Zhang, W. Li, C. X. Zhang, B. X. Han, *Chem. Commun.* **2009**, *17*, 2365–2367.
[25] K. Ghosh, H. J. Lehmler, S. E. Rankin, B. L. Knutson, *J. Colloid Interface Sci.* **2012**, *367*, 183–192.
[26] C. Palocci, A. Barbetta, A. L. Grotta, M. Dentini, *Langmuir* **2007**, *23*, 8243–8251.
[27] J. Ming, Y. Q. Wu, L. Y. Wang, Y. C. Yu, F. Y. Zhao, *J. Mater. Chem.* **2011**, *21*, 17776–17782.
[28] J. W. Wang, Y. D. Xia, W. X. Wang, M. Poliakoff, R. Mokaya, *J. Mater. Chem.* **2006**, *16*, 1751–1756.
[29] J. M. Sun, C. L. Wang, L. Wang, L. Liang, X. F. Liu, L. Chen, F. S. Xiao, *Catal. Today* **2010**, *158*, 273–278.
[30] M. M. J. Treacy, J. B. Higgins, *Collection of Simulated XRD Powder Patterns for Zeolites*, Elsevier, New York, **1996**, pp. 352–354.
[31] F. T. Fan, Z. C. Feng, K. J. Sun, M. L. Guo, Q. Guo, Y. Song, W. X. Li, C. Li, *Angew. Chem. Int. Ed.* **2009**, *48*, 8743–8747; *Angew. Chem.* **2009**, *121*, 8899.
[32] Z. Y. Yuan, T. Z. Ren, B. L. Su, *Chem. Phys. Lett.* **2004**, *383*, 348–352.
[33] H. W. Liu, M. Z. Yates, *Langmuir* **2003**, *19*, 1106–1113.
[34] J. Li, X. Li, Y. Shi, D. S. Mao, G. Z. Lu, *Catal. Lett.* **2010**, *137*, 180–189.
[35] H. L. Ren, F. Xin, *Catal. Commun.* **2006**, *7*, 848–854.
[36] P. L. Zhang, L. Wang, L. M. Ren, L. F. Zhu, Q. Sun, J. Zhang, X. J. Meng, F. S. Xiao, *J. Mater. Chem.* **2011**, *21*, 12026–12033.
[37] D. C. Cheng, X. X. Zhao, F. Q. Chen, X. L. Zhan, *Catal. Commun.* **2009**, *10*, 1450–1453.
[38] R. H. Zhao, M. Dong, Z. F. Qin, J. G. Wang, *Mater. Lett.* **2008**, *62*, 4573–4575.
[39] L. G. Hortiguela, C. M. Alvarez, E. Sastre, F. Cora, J. P. Pariente, *Catal. Today* **2006**, *114*, 174–182.
[40] W. L. Dai, W. B. Kong, G. J. Wu, N. Li, L. D. Li, N. J. Guan, *Catal. Commun.* **2011**, *12*, 535–538.
[41] L. H. Zhuo, Y. Q. Wu, L. Y. Wang, J. Ming, Y. C. Yu, X. B. Zhang, F. Y. Zhao, *J. Mater. Chem.* **2013**, *1*, 3594–3960.
[42] C. S. Park, K. S. Kim, Y. J. Park, *J. Power Sources* **2013**, *244*, 72–79.
[43] L. P. Zhou, J. Xu, C. Chen, F. Wang, X. Q. Li, *J. Porous Mater.* **2008**, *15*, 7–12.
[44] W. B. Fan, A. S. Robert, M. W. Bert, *Phys. Chem. Chem. Phys.* **2001**, *3*, 3240–3246.

Received: February 15, 2014
Published Online: May 20, 2014

